JCTC Journal of Chemical Theory and Computation

Article

pubs.acs.org/JCTC

Tailoring Pull-out Properties of Single-Walled Carbon Nanotube Bundles by Varying Binding Structures through Molecular Dynamics Simulation

Liuyang Zhang and Xianqiao Wang*

College of Engineering and NanoSEC, University of Georgia, Athens, Georgia 30602, United States

ABSTRACT: Single-walled carbon nanotubes (SWCNTs) have demonstrated a remarkable capacity for self-assembly into nanobundles through intermolecular van der Waals interactions, bestowing these agglomerates extraordinary mechanical, thermal, and electrical properties. However, how to improve the binding ability of SWCNT bundles to mitigate the delamination and sliding effects between individual nanotubes remains to be further investigated. By utilizing molecular dynamics simulation, here we present the construction of SWCNT bundles with discrete cylindrical and continuous helical binders by noncovalent coating of the bundle surface with sp^2-hybridized carbon networks. Meanwhile, by modifying the binding potentials between the binder and SWCNT bundles to mimic the different binding types actually used, the bound SWCNT bundle presents a variety of distinct mechanical properties unmatched by unbound bundles. The pull-out tests with discrete binders portray an intriguing force−displacement curve which can help determine the number of discrete binders used in the system. SWCNT bundles with binders depict unique mechanical properties which can differentiate them from unbound SWCNT bundles. These findings provide compelling evidence that bound SWCNT bundles will open up novel avenues for a variety of applications, especially in nanocomposites.

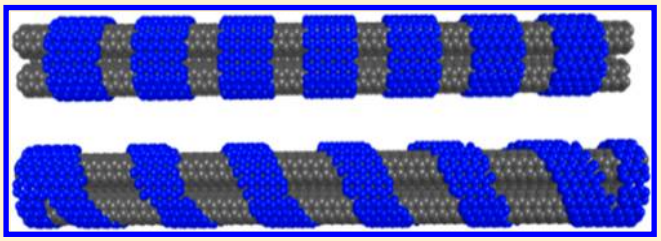

1. INTRODUCTION

Since the discovery of single-walled carbon nanotubes (SWCNTs), a large amount of work has been reported on the extraordinary electrical,[1−3] mechanical,[4] and thermal properties[5−7] of these structures. SWCNTs have showed the ability to self-assemble into crystalline bundles composed of vertically aligned carbon nanotubes (CNTs),[8,9] which enhance the potential applications of CNTs. For example, CNT bundles are potentially adopted as reinforcing elements for strong but flexible composite materials. Many studies have been carried out either theoretically or via computational modeling of CNT bundles on their distinct properties. For instance, the structural transformation of CNT bundles is revealed to be closely related to the diameter and symmetry of the individual CNTs in the bundles by means of density functional theory calculations.[10] The cross sections of CNTs switch from circular to hexagonal due to changes in the tube diameter and the externally applied pressure. This shift leads to structural instability and an abrupt change of the elastic properties of the CNT bundles.[11] The bundling of CNTs further lowers the energy gap in semiconducting CNTs and therefore significantly broadens the density of states and optical absorption bands.[12] The buckling load of CNT bundles is directly proportional to the loading capacity of the single SWCNTs, and the intratubular van der Waals (vdWs) force plays an important role in strengthening the overall rigidity of the CNT bundles.[13] The critical buckling/failure loads and the corresponding compressive/tensile strains of twisted CNT bundles are obtained for both axial compression and tension scenarios, and the findings show that an increase in the twisting angle causes dramatically decreased properties.[14] The force required to pull out an inner bundle of double-walled carbon nanotubes (DWCNTs) from an outer shell of DWCNTs has been measured as 1.7 ± 1.0 nN using in situ scanning electron microscopy methods.[15] With the inclusion of a binding polymer, the effect of the noncovalently adsorbing cross-links on the improvement of CNT bundle properties has been explored for the development of viable polymer-reinforced CNT composites.[16] Based on the electrostatic capacitive force and intratubular vdWs interaction, the middle CNT inside the bundle oscillates at a frequency controlled by the size and length of the CNT.[17,18]

Appreciable efforts have been devoted toward the study of carbon nanotube bundles as seen from the above discussion; however, there is still a lack of understanding in how to enhance the binding ability of SWCNT bundles in order to mitigate the delamination and sliding effect between the nanotubes due to the inherent properties of long ratio aspect SWCNTs. In this paper, by introducing unique discrete or continuous binders on the outer surface of a SWCNT bundle, the bundle will demonstrate the cooperative behaviors unmatched by unbound SWNCT bundles. By performing the pull-out and tensile mechanical test with molecular dynamics simulation, we will demonstrate that the mechanical properties

Received: February 19, 2014
Published: June 12, 2014

   dx.doi.org/10.1021/ct5001473 | J. Chem. Theory Comput. 2014, 10, 3200−3206

of SWCNT bundles can be tailored by the type and density of varying binders. The binder provides an intriguing way for the bundles to form complex structures and also serves to manipulate their mechanical properties. Our findings will provide an interesting look at novel nanostructures and shed light on the fabrication and application of CNT-based nanocomposite materials.

2. COMPUTATIONAL MODEL AND METHODOLOGY

In order to model bond formation and breaking in the simulation system, we have used the adaptive intermolecular reactive empirical bond order (AIREBO) potential.[19] It should be noted that this potential is best suited for systems containing only hydrogen and carbon atoms, which makes it accessible for all-carbon systems such as the ones being employed here. The AIREBO potential can be expressed as

$$E = \frac{1}{2}\sum_{i}\sum_{j\neq i}\left[E_{ij}^{\mathrm{REBO}} + E_{ij}^{\mathrm{LJ}} + \sum_{k\neq i,j}\sum_{l\neq i,j,k} E_{kijl}^{\mathrm{TORSION}}\right] \quad (1)$$

where the E^{REBO} term is the REBO potential,[20] shown as

$$E_{ij}^{\mathrm{REBO}} = V_{ij}^{\mathrm{R}}(r_{ij}) + b_{ij}V_{ij}^{\mathrm{A}}(r_{ij}) \quad (2)$$

where V^{R} is a repulsive term, V^{A} is an attractive term, and b_{ij} is the environmental-dependent bond order term between atoms which activates the attractive term only for bonded atoms. Since the REBO potential only accounts for interactions of atoms within two angstroms of one another, the AIREBO potential also includes the E_{LJ} term, which is a standard 12-6 Lennard-Jones potential for distances 2 Å < r < cutoff.

$$E_{\mathrm{LJ}} = 4\epsilon\left[\left(\frac{\sigma}{r}\right)^{12} - \left(\frac{\sigma}{r}\right)^{6}\right] \quad (3)$$

where ϵ is the depth of potential well, σ is the finite distance where the potential is zero, and r is the distance between the particles. The cutoff for the LJ term is set here to be 2.5σ as a good balance between computational speed and accuracy. The AIREBO potential also includes the E^{TORSION} term, which is a four-body potential describing hydrocarbon dihedral angle preference. The conjugate gradient algorithm is employed to perform the energy minimization until the total energy change between two successive iterations divided by the energy magnitude is less than or equal to 10^{-8}. After this equilibrium state is achieved, NVT ensemble simulations with a constant temperature of 1 K are carried out based on the Berendsen thermostat and Newtonian equations of motion. To mitigate the influence of the damping component in the thermostat on the adhesive forces, we have adopted a very low temperature to make sure that the temperature influence is minimal and can be negligible. The time step used for MD simulation is 0.1 fs. The simulations last around 12−14 ps. All the simulations are performed with the LAMMPS package.[21]

In this paper, the investigated SWCNT bundle is composed of three parallel SWCNTs with chirality (3,3) oriented longitudinally along the z-axis with a length of 14.7 nm and with a cross section as depicted in Figure 1. The number of atoms in three parallel SWCNTs is 2160. The intertubular distance is about 3.4 Å, and the intertubular interaction is described by a 12-6 Lennard-Jones potential with σ = 3.367 Å and ϵ = 4.555 meV as has been previously demonstrated for the testing of the tensile and compressive properties of CNT bundles.[22] Two kinds of binders are proposed to reinforce the bundle: discrete cylindrical binders and a continuous helical binder. The noncovalent interaction between the binders and the bundle is also described by a 12-6 LJ potential, but here we have varied the parameters to mimic different binding strengths. By using three (3,3) SWCNTs, we intend to maximize the relative contact areas between the binder and the bundle for better understating the effect of adhesive forces from binders on the integral function of the SWCNT bundle. Also strong binding strength leads to the wrinkle of binders to further the contact area. With respect to more SWCNTs in the bundle, the relative contact areas decrease and the binding interaction is weakened. Also for larger diameter SWCNTs, as anticipated, they experience the similar decrease of contact areas and weakened binding interactions. We perform a series of pull-out and tensile mechanical tests to investigate the mechanical properties of bundles with these two kinds of binders. Following equilibration, steered molecular dynamics (SMD)[23] in the form of a constant velocity (0.1 Å/ps) in the z direction is applied to the center SWCNT of each bundle through a virtual spring attached to dummy atoms. The force F acting on the dummy atoms during displacement to an imaginary point can be calculated by the following equations:

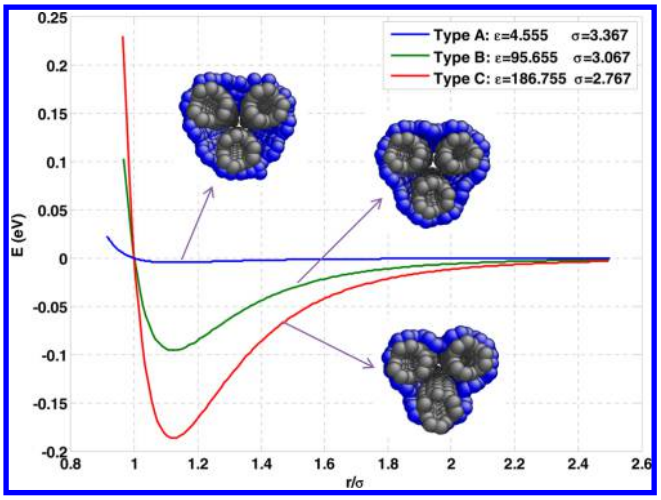

Figure 1. Three different types of binding potentials between the SWCNT bundle and the binder. The carbon atom in blue shows the outside binder, while the gray shows the inner bundle.

$$F = -\nabla U \quad (4)$$

$$U = \frac{1}{2}k[vt - (r - r_0)\cdot n]^2 \quad (5)$$

where ∇U is the potential energy gradient, k is the spring force constant, v is the velocity of pulling process, t is the current time, r is the instantaneous vector position, r_0 is the initial vector position of the SMD atom, and n is the vector direction in which the dummy atom is displaced.

3. RESULTS AND DISCUSSION

3.1. Binding Potentials. To overcome the weak intertubular vdWs interaction and improve the stability of CNT bundles for mechanical applications, we introduce a mechanical enhancer, or binder, to improve the cooperative ability of SWCNT bundles and also mitigate the sliding and delamination effects which can lead to the catastrophic failure of the whole structure. Before we investigate the properties of various binders, however, it will be intriguing to unravel the effect of

dx.doi.org/10.1021/ct5001473 | J. Chem. Theory Comput. 2014, 10, 3200−3206

the binding capability between the SWCNTs and binders on the sliding behavior of the system. As expected, the binding interaction between the binder and the bundles enforces the bundle to act as a single structure and at the same time introduces friction between the binder and bundle. To demonstrate the different binding ability of the binders, from the perspective of model materials, we adjust the long-range LJ parameter to mimic the interaction encountered in fiber composites.[24−26] A variation in the binding potential can be achieved in several ways[27,28] which accounts for the differences in the adhesion force between binders and the bundles. Here, three pairs of σ and ϵ are adopted to control the attractive interaction between binder and bundle in the simulation, as shown in Figure 1. The LJ potentials used in this study are type A with σ = 3.367 Å and ϵ = 4.555 meV, type B with σ = 3.067 Å and ϵ = 95.655 meV, and type C with σ = 2.767 Å and ϵ = 186.755 meV. Type B and type C are chosen to increase the binding force only for the purpose of comparison and demonstration, which are the "model materials" and cannot be found in the literature yet. After energy minimization, the binder adheres to the surface of the bundle with different strength and conformation dependent on the binding potential used. With the low LJ parameters (type A), the binder has weak interaction with the bundle and thus adheres rather loosely, with a minimal increase in packing density of the bundle. With the strong LJ potential (type C), the space between the SWCNTs around the outside surface of the bundle is filled by the binders and the bundle is firmly compressed by the binders, and the bundle is also slightly deformed along the axial direction. The adjustable LJ binding potential provides the platform to employ the following series of mechanical tests for investigating the performance of the bundle with different types of binders.

3.2. Pull-out Tests with Discrete Cylindrical Binders. To improve the integrity and stability of the CNT-based nanocomposite structures, the cylindrical binder is the most suitable choice to maintain a radially symmetric configuration, as each SWCNT is being exposed to an almost identical circumferential force by the cylindrical binder. The cylindrical CNT strip serves as an excellent candidate when choosing the binders. Besides, the CNT-like binder is feasible and convenient for the modeling, and it also has mature AIREBO potential to describe the interaction between the binder and bundle. The model will experience the AA/AB stacking transition due to interaction between this special CNT binders and SWCNT bundle, although it does not affect the main objective of our study—how to improve the performance of carbon nanotube bundles. The cylindrical binder is constructed from a segment of SWCNTs with (11,11) chirality, which is determined to be approximately equal to the circular radius of the cross section of the bundle. The diameter of the binder can be calculated from the (n,m) indices by $d = a/\pi(n^2 + nm + m^2)^{1/2}$, where a = 0.246 nm. The cylindrical binder keeps a minimum distance of 3.4 Å away from the outside wall of each SWCNT since this is the traditional width of interlayer spacing in sp^2 carbon materials.

We first examine how the binding potential affects the behavior of pull out of a single SWCNT from the bundle. Figure 2 shows the relationship of the pull-out force and displacement of a single SWCNT from the 3-SWCNT-based bundle with no binders and with cylindrical binders utilizing the type A, type B, and type C binding potentials. It is also noticed that the maximum magnitude of the pull-out force is around 1.5 nN, which is in good agreement with the results from double-walled CNT pull-out test.[15] It is evident that the traditional stick−slip behavior is observed, which appreciably emanates from the energy gap between the AA and AB stacking of carbon atoms on the CNT surfaces. Figure 2 describes the evolution of the pull-out force versus the displacement which the extracted SWCNT experiences in a bundle with seven discrete cylindrical binders under three different types of binding potential, with an extraction test with no binders for comparison. Seven discrete cylindrical binders with individual length of 11.10 Å are uniformly distributed along the axial direction of the bundle with a gap spacing of 8.95 Å. The number of atoms in the 7-binder is 1540. During the SMD simulation, one end of a SWCNT is attached to the spring while the end of the other two SWCNTs at the side opposite to the pull-out direction is constrained in the z direction. The binders are also constrained in the z direction during the pull-out test to avoid sliding on the surface of the SWCNT. Figure 2 highlights the characteristic zigzag force−displacement curve of the single carbon nanotube pull out from the bundles. It is notable that this curve can serve as a unique signature to distinguish the number of binders in a specific bundle system. The maximum amplitude of pull-out force with the type A binding potential in this case is around 12 nN, which is close to 8 times higher than the force in the same bundle without binders. During the process of the pull-out test, the force experiences the intrinsic seven large jumps no matter what kind of binding potential we have adopted. This unique phenomenon can be explained as follows: when the end of the SWCNT passes through the edge of a binder, the interaction

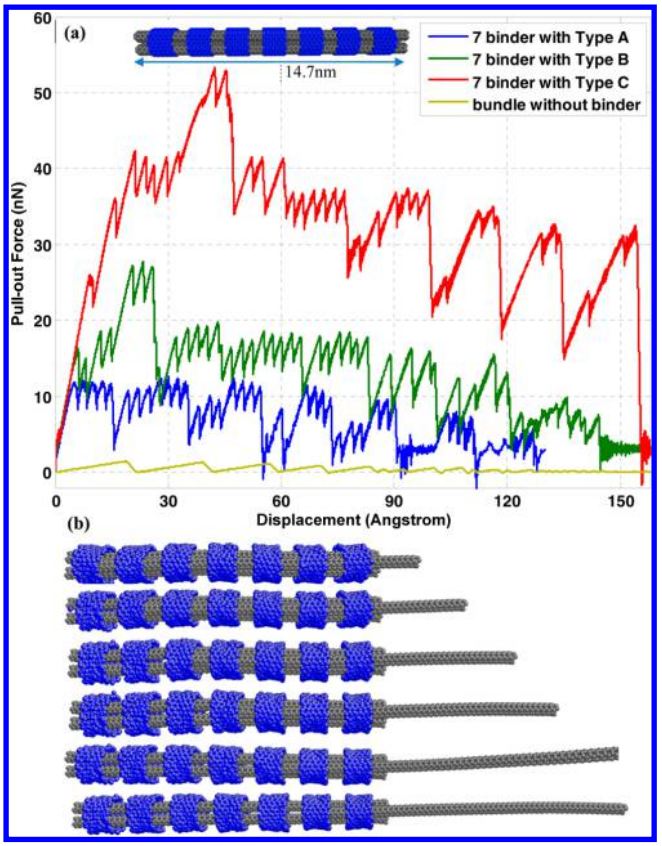

Figure 2. (a) Pull-out force and displacement relationship of a 7-binder SWCNT bundle with three binding potential types A, B, and C depicted in Figure 1. (b) Evolution of the pull-out process of a single CNT from the bundle.

from this binder will dramatically drop and fade away in accordance with the distance they separate. In each large jump of the force curve, there exist a number of small zigzag fluctuations triggered by the mismatch switch AA/AB stacking of carbon atoms between the binder and the surface of the CNT. Meanwhile, with the increase of binding potentials from type A to type C, as expected, the average pull-out force increases tremendously due to the augmentation of intermolecular force between the binders and the bundle.

When structures or material systems scale down to nanometer size, surface effects have been shown to play a key role in determining the properties or behaviors of the system of interest. Contact splitting into finer contact elements results in stronger adhesion for several independent reasons, such as adaptability to rough surfaces, uniform stress distribution, defect control, and adhesion redundancy, etc.[29] The adaptability to the rough surface of SWCNTs is obvious while we divide the same length of binder into 3, 6, and 9 discrete binders and put them outside the bundle. An intriguing question arises: how does the bundle behave if the total length of binders along the axial direction is kept the same while the number of equally spaced identical binders is varied? To tackle this tantalizing enigma, cylindrical binders with a total length of 85 Å are partitioned into 3 and 6 segments, as depicted in Figure 3, and 9 segments in Figure 4. All cylindrical binders

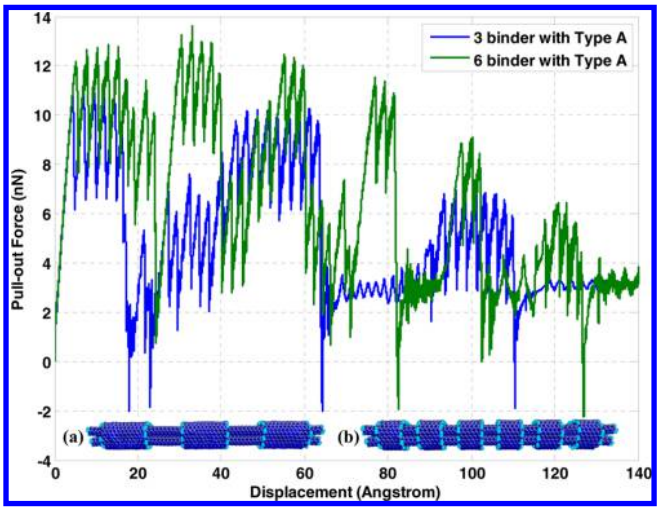

Figure 3. Comparison of pull-out force between 3-binder and 6-binder SWCNT bundles. (a) Atomic potential map of 3-binder bundle; (b) atomic potential map of 6-binder bundle. The potential energy varies from −7.472 eV (dark blue) to 0 eV (dark red). The average of potential energy of edge carbon atoms is −4.97 eV (light blue).

used in a single run are of equal length and spacing and use the same potential. The number of atoms in 3-, 6-, and 9-binders are almost identical, 1584. Type A binding potential is adopted in the simulation, and the center-to-center distance between any two neighboring binders for the 3-, 6-, and 9-binder SWCNT bundle is 50, 22.8, and 14.75 Å, respectively. The pull-out force−displacement curve in Figure 3 portrays the similar feature demonstrated in Figure 2—the number of large jumps on the curve for each specific bundle is equal to the number of binder segments it possesses. From Figure 3, it is also observed that the maximum pull-out force increases from 10 pN for the 3-binder bundle to 12 pN for the 6-binder bundle. This phenomenon can be attributed to the edge effect which the binders exert on the surface of the bundle as evidenced by the

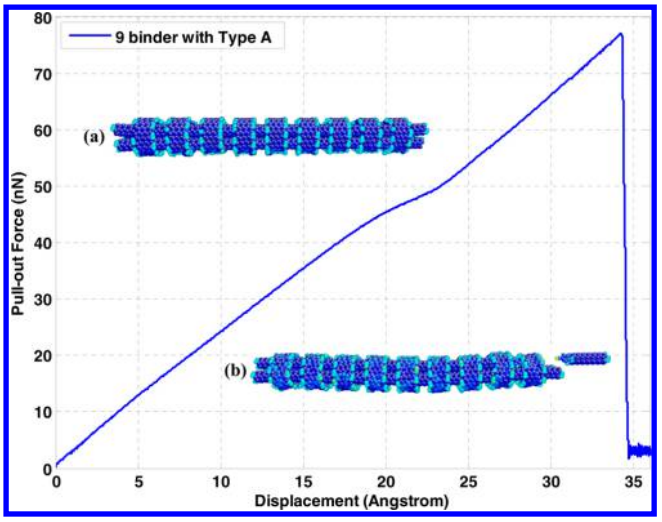

Figure 4. Pull-out simulation of a SWCNT bundle with 9 cylindrical binders. (a) Atomic potential map of 9-binder bundle; (b) atomic potential map of 9-binder bundle at breaking point. The potential energy varies from −7.822 eV (dark blue) to 0 eV. The average of potential energy of edge carbon atoms is −5.02 eV (light blue).

potential energy maps shown in Figure 3a,b. In other words, the number of carbon atoms exposed on the edge of binders affects the binding energy between binder and bundle; therefore, more edge carbons lead to an overall increase in force between the binders and bundle. With respect to 9-binder SWCNT bundle shown in Figure 4, the extraction process fails because the astounding strength (78 nN) of the binder−bundle interaction exceeds the tensile strength of a single CNT. Compared with the pull-out simulation of multiwalled CNT[30] in which the inner SWCNT is regarded as completely covered with a binder, however, the extraction force of a CNT bundle with discrete binders is larger. It is also observed in Figure 4 that the curve of force−displacement demonstrates unusual smoothness compared with the results from Figure 3, which can be explained by lack of relative sliding between the binders and bundle, engendering almost no switching between AA and AB stacking of carbon atoms. To summarize, these findings provide a novel avenue to tailor the pull-out behavior of SWCNT bundles via the number of discrete binders on the surface of the system.

3.3. Pull-out Test with Helical Binder. In what follows, inspired by the strong effects of the number of binders, we further investigate the pull-out behavior of a bundle with a continuous helical binder to achieve a SWCNT bundle with desired properties. A single continuous helical binder wraps the entire bundle uniformly along the axial direction, similar to DNA wrapping on a CNT,[31] as shown in Figure 5. The helical binder is constructed from a SWCNT with (11,11) chirality. The contact area between the helical binder and bundle depends on the defined angle between the plane of the cross section and wrapping direction. The width of the helical binder is a constant 9.77 Å, and the angle is chosen as 33.7°. We perform the pull-out test to investigate the binding effect of this continuous binder. The pull-out force in Figure 5 is dominated by successive jumps decreasing in magnitude. To make a comparison between the two types of binder, in Figure 6, we construct a continuous helical binder with an angle of 23.4° and a width of 9.77 Å, which has the same effective area as the 7 cylindrical binders in Figure 2. Under the type A binding

dx.doi.org/10.1021/ct5001473 | J. Chem. Theory Comput. 2014, 10, 3200−3206

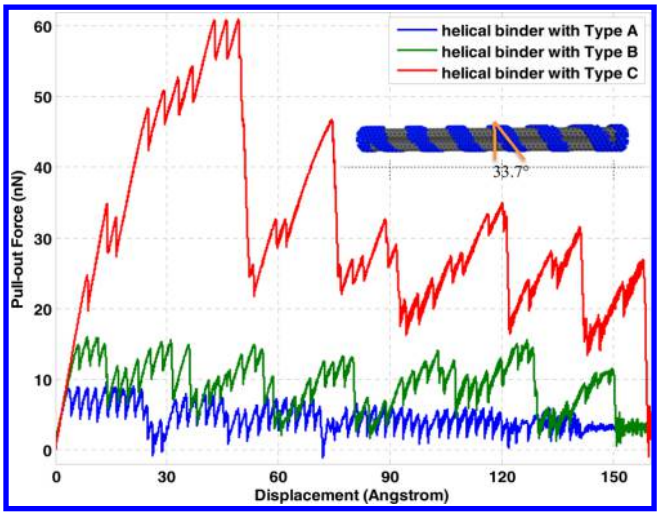

Figure 5. Pull-out force and displacement relationship of the SWCNT bundle with helical binders under three binding potentials, types A, B, and C, as depicted in Figure 1

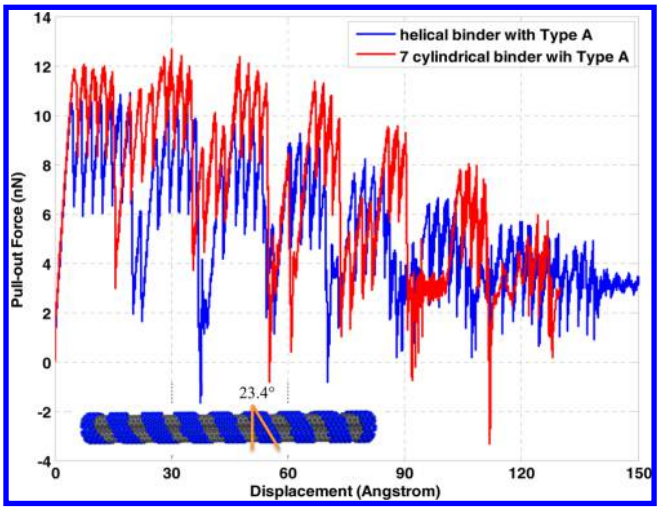

Figure 6. Comparison of the pull-out force between bundles with discrete binders and helical binders. Both binders have the same effective binding area.

potential, the bundle with 7 cylindrical discrete binders performs better than the one with helical binder as far as the pull-out force is concerned. From the viewpoint of energy map in graphene layers, the interaction energy caused by the AB stacking of carbon atoms between the two neighboring layers possesses the lowest value among all the orientations while the AA stacking creates the highest value. The energy gap between the AA and AB stacking formations is 0.36mev/atom.[32] The bundle with the helical binder possesses a mixed model of AA and AB stacking orders while the bundle with 7 cylindrical discrete binders has the pure AA stacking at the initial configuration, which leads to the subtle difference in pull-out behaviors.

3.4. Tensile Test. Due to the weak van der Waals interaction between individual CNTs in the bundle which render them able to rotate and slide relative to each other, the CNT bundles have reflected lower elastic moduli when compared with individual SWCNTs.[33] Therefore, an interesting question arises: can the binder enhance the integral property of the SWCNT bundle? To unveil the mystery, we perform tensile tests with three different configurations of SWCNT bundles, as depicted in Figure 7. During the simulation, for all cases, one

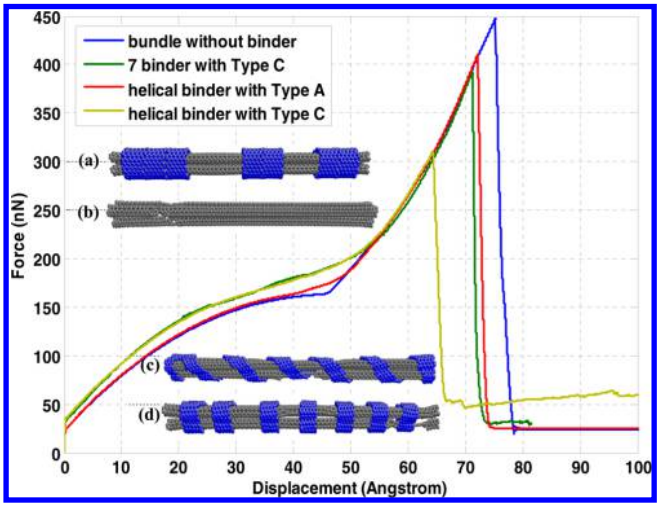

Figure 7. Tensile performances of SWCNT bundles with 7-binder and helical binder combining with different types of binding potentials. (a) Snapshot of aggregation of 7-binder with type A potential. (b–d) Snapshots of each case at the breaking point.

end of the bundle with a length of 10 Å is fixed while the other end of the bundle with the same length is treated as a rigid body and tethered to a virtual spring in order to apply a constant displacement boundary condition. From the simulation results, it is noticed that, irrespective of the cases once one of the individual SWCNTs breaks, the total force on the bundle is supported only by the other SWCNTs and thus triggers a domino effect toward catastrophic failure of the bundle. This is in perfect agreement with the brittle properties of CNTs at high strain and low temperature.[34] For the seven cylindrical discrete binders, we adopt the type C binding potential to ensure that the binder is closely attached to the bundle and fails to move during the test due to the tensile deformation of the bundle. Type A binding potential leads to the aggregation of all of the cylindrical discrete binders along the bundle, as shown in Figure 7a. The figure also shows that the high binding potential for both continuous helical and discrete cylindrical binders makes the bundle easier to break when compared with the bundle with no binders. The stress on the cylindrical binder with type C potential is estimated as 3.58 GPa. The yield force of the unbound bundle reaches 450 nN, while in the other cases, failure occurs at smaller forces. Owing to the asymmetrical effect of helical binder, the bundle twists and conforms to the same pattern as the helical binder. In contrast to the theory of wire ropes in continuum mechanics, the twisted CNT bundles do not exhibit better tensile properties[14] as is observed in twisted wire ropes. The twisting effect lowers the intertubular distance, which leads to an increase in the repulsive energy between the individual SWCNTs and subsequently creates increased residual stresses. The stress on the helical binder with type A potential is estimated as 1.73 GPa, while with type C potential the stress is estimated as 3.0 GPa. Therefore, the SWCNT bundles with high binding potential binders tend to fail at junctions while under lower loads when compared with unbound bundles. SWCNT bundles with high binding potential binders (discrete or continuous) can be viewed as equivalent bundles with shear residual force along the radial direction and/or with bending

dx.doi.org/10.1021/ct5001473 | J. Chem. Theory Comput. 2014, 10, 3200–3206

force along the axial direction. These factors eventually lead to the counterintuitive performance, lowering the yield force of the SWCNT bundles with binders. For the tensile test, with larger SWCNTs in the bundle, the bundle exhibits higher failure loads; however, it is also evident that the average failure load of each SWCNT in a CNT bundle of three is very close to that of a CNT bundle of seven.[22] It can therefore be deduced that the critical failure loads for CNT bundles are directly proportional to the average critical failure load of each SWCNT in the CNT bundle, which allows simple computation of CNT bundles of up to hundreds of SWCNTs without having to perform computationally expensive MD simulations with millions of atoms. Besides, the critical failure loads follow a linear relationship with respect to the diameters of each SWCNT in the CNT bundles, which enables the determinations of critical failure loads of other sizes of CNT bundles by simply extrapolating the data.

Through the tensile test, either a discrete cylindrical binder or a helical binder has prominent effects on the SWCNT bundle. To deeply appreciate the benefit from binders to improve the performance of CNT bundles, a discontinuous bundle is constructed to make a better comparison of tensile strength due to binders. Recently high-performance synthetic fibers have been under development by achieving the alignment of carbon nanotubes with the fiber axis.[35] However, the defects at random intervals are associated with local deficiencies in densification which would attenuate the stress transfer between the CNT within bundles. To enhance the mechanical properties of fiber with defects, 7 cylindrical binder and helical binder is applied to the discontinuous bundle (SWCNT does not span from one end to the other). The discontinuous bundle is achieved by cutting each SWCNT into two parts at random position, as shown in Figure 8a. The tensile simulation for a discontinuous bundle without any binder is similar to the single SWCNT pull out from the bundle, as shown in Figure 3, but

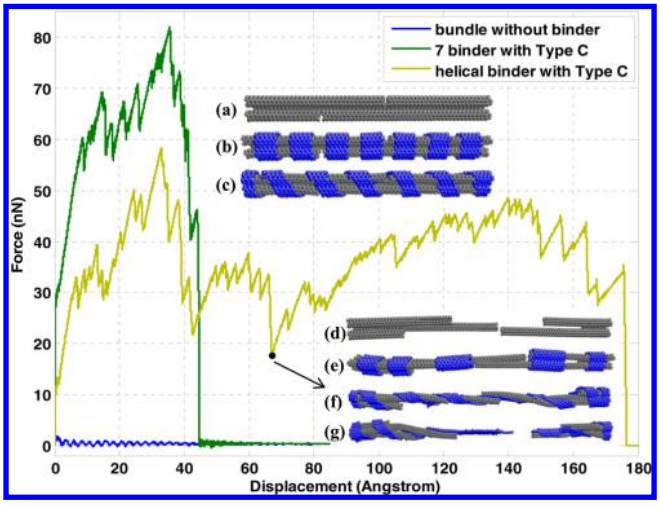

Figure 8. Tensile performances of discontinuous SWCNT bundles with 7-binder and helical binder combined with type C binding potential. (a) snapshot of initial discontinuous bundle in which each SWCNT is cut into two parts at a random position. (b) Snapshot of initial discontinuous bundle as (a) but with 7-binder. (c) Snapshot of initial discontinuous bundle as (a) but with a helical binder. (d) Final snapshot of the discontinuous bundle. (e) Final snapshot of discontinuous bundle with 7-binder. (f) Snapshot of discontinuous bundle with a helical binder when the helical binder is pulled. (g) Final snapshot of discontinuous bundle with a helical binder.

the pull-out force is extremely small, indicating that there is almost no interaction between the discrete SWCNTs. With discrete cylindrical binder with type C potential, the yield force is 82.03 nN, which shows that the strength of the bundle is significantly improved. The similar aggregation of the cylindrical binder is observed during the tensile test as explained in Figure 7. For the helical binder, the yield force is 58.35 nN, which is smaller but comparable to that of 7-binder as the helical binder twists the discontinuous bundle. Figure 8f shows that the helical binder sustained the load when the deformation is about 45.7%, where the SWCNT has no contact area any more. No stress could be transferred by the shear between the SWCNTs. It also should be noticed that the continuous helical binder keeps the bundle as a whole all the way to 120% deformation, where the helical binder breaks down. The two types of binders demonstrate the capability to effectively transfer the load from one to another SWCNT of the discontinuous bundle, which can be unachievable without any binder. By the tensile test of the continuous and discontinuous SWCNT bundle, it shows that binders are not necessary to provide the supportive effort as we expected in the continuous bundles at macroscale; however, it could help to enhance the mechanical properties of a discontinuous bundle.

4. CONCLUDING REMARKS

In this paper, we have performed molecular dynamics simulations to introduce two types of single-walled carbon nanotube bundles by constructing cylindrical discrete binders as well as continuous helical binders. In addition, we investigate the pull-out behavior and tensile properties of the bundles to fully unravel the mechanisms behind these behaviors. Simulation results have demonstrated that the binders play a significant role in affecting the pull-out behavior of the SWCNT bundle. The binding effect can be manipulated by controlling the LJ potential between the binder and bundle, therefore offering a promising way to design the nanotube bundles with programmable pull-out properties. Also, the pull-out force–displacement curves of the SWCNT bundles bound with cylindrical binders possess unique signatures which distinguish the number of binders. The bundles with helical binders have lower elastic properties due to the twisting effect of the binder. Binders have demonstrated the invaluable capability to effectively transfer the stress between discrete carbon nanotubes in a discontinuous bundle, therefore greatly enhancing the tensile strength and flexibility of CNT bundles. These findings in this paper provide computational guidelines to study the binding effect of bound CNT bundles and the mechanical properties of the CNT-based composite materials.

AUTHOR INFORMATION

Corresponding Author

*Tel: 706-542-6251. E-mail: xqwang@uga.edu.

Funding

The authors acknowledge support from the National Science Foundation (Grant No. CMMI-1306065) and University of Georgia (UGA) startup fund.

Notes

The authors declare no competing financial interest.

■ ACKNOWLEDGMENTS

The facility support for modeling and simulations from the UGA Advanced Computing Resource Center is greatly appreciated.

■ REFERENCES

(1) Bandaru, P. R. Electrical properties and applications of carbon nanotube structures. *J. Nanosci. Nanotechnol.* **2007**, *7* (4−5), 1239−1267.
(2) Odom, T. W.; Huang, J.-L.; Kim, P.; Lieber, C. M. Structure and Electronic Properties of Carbon Nanotubes. *J. Phys. Chem. B* **2000**, *104* (13), 2794−2809.
(3) Odom, T. W.; Huang, J.-L.; Kim, P.; Lieber, C. M. Atomic structure and electronic properties of single-walled carbon nanotubes. *Nature* **1998**, *391* (6662), 62−64.
(4) Ruoff, R. S.; Qian, D.; Liu, W. K. Mechanical properties of carbon nanotubes: theoretical predictions and experimental measurements. *C. R. Phys.* **2003**, *4* (9), 993−1008.
(5) Hone, J.; Llaguno, M. C.; Biercuk, M. J.; Johnson, A. T.; Batlogg, B.; Benes, Z.; Fischer, J. E. Thermal properties of carbon nanotubes and nanotube-based materials. *Appl. Phys. A: Mater. Sci. Process.* **2002**, *74* (3), 339−343.
(6) Lukes, J. R.; Zhong, H. Thermal conductivity of individual single-wall carbon nanotubes. *J. Heat Transfer* **2006**, *129* (6), 705−716.
(7) Ren, C.; Zhang, W.; Xu, Z.; Zhu, Z.; Huai, P. Thermal conductivity of single-walled carbon nanotubes under axial stress. *J. Phys. Chem. C* **2010**, *114* (13), 5786−5791.
(8) Thess, A.; Lee, R.; Nikolaev, P.; Dai, H.; Petit, P.; Robert, J.; Xu, C.; Lee, Y. H.; Kim, S. G.; Rinzler, A. G.; Colbert, D. T.; Scuseria, G. E.; Tománek, D.; Fischer, J. E.; Smalley, R. E. Crystalline ropes of metallic carbon nanotubes. *Science* **1996**, *273* (5274), 483−487.
(9) Journet, C.; Maser, W. K.; Bernier, P.; Loiseau, A.; de la Chapelle, M. L.; Lefrant, S.; Deniard, P.; Lee, R.; Fischer, J. E. Large-scale production of single-walled carbon nanotubes by the electric-arc technique. *Nature* **1997**, *388* (6644), 756−758.
(10) Zhao, X.; Zhang, K.; Wang, J.; Duan, H. Structural transformation of single wall carbon nanotube bundles under pressure. *Math. Mech. Solids* **2010**, *15* (7), 744−754.
(11) Liu, J.; Zheng, Q.; Wang, L.; Jiang, Q. Mechanical properties of single-walled carbon nanotube bundles as bulk materials. *J. Mech. Phys. Solids* **2005**, *53* (1), 123−142.
(12) Reich, S.; Thomsen, C.; Ordejón, P. Electronic band structure of isolated and bundled carbon nanotubes. *Phys. Rev. B* **2002**, *65* (15), 155411.
(13) Liew, K. M.; Wong, C. H.; Tan, M. J. Buckling properties of carbon nanotube bundles. *Appl. Phys. Lett.* **2005**, *87* (4), 041901-3.
(14) Liew, K. M.; Wong, C. H.; Tan, M. J. Twisting effects of carbon nanotube bundles subjected to axial compression and tension. *J. Appl. Phys.* **2006**, *99* (11), 114312-7.
(15) Filleter, T.; Yockel, S.; Naraghi, M.; Paci, J. T.; Compton, O. C.; Mayes, M. L.; Nguyen, S. T.; Schatz, G. C.; Espinosa, H. D. Experimental−computational study of shear interactions within double-walled carbon nanotube bundles. *Nano Lett.* **2012**, *12* (2), 732−742.
(16) Bratzel, G. H.; Cranford, S. W.; Espinosa, H.; Buehler, M. J. Bioinspired noncovalently crosslinked "fuzzy" carbon nanotube bundles with superior toughness and strength. *J. Mater. Chem.* **2010**, *20* (46), 10465−10474.
(17) Kang, J. W.; Song, K. O.; Hwang, H. J.; Jiang, Q. Nanotube oscillator based on a short single-walled carbon nanotube bundle. *Nanotechnology* **2006**, *17* (9), 2250.
(18) Cox, B. J.; Thamwattana, N.; Hill, J. M. Mechanics of nanotubes oscillating in carbon nanotube bundles. *Proc. R. Soc. A* **2008**, *464* (2091), 691−710.
(19) Stuart, S. J.; Tutein, A. B.; Harrison, J. A. A reactive potential for hydrocarbons with intermolecular interactions. *J. Chem. Phys.* **2000**, *112* (14), 6472−6486.
(20) Donald, W. B.; Olga, A. S.; Judith, A. H.; Steven, J. S.; Boris, N.; Susan, B. S. A second-generation reactive empirical bond order (REBO) potential energy expression for hydrocarbons. *J. Phys.: Condens. Matter* **2002**, *14* (4), 783.
(21) Plimpton, S. Fast Parallel Algorithms for Short-Range Molecular Dynamics. *J. Comput. Phys.* **1995**, *117* (1), 1−19.
(22) Liew, K.; Wong, C.; Tan, M. Tensile and compressive properties of carbon nanotube bundles. *Acta Mater.* **2006**, *54* (1), 225−231.
(23) Izrailev, S.; Stepaniants, S.; Isralewitz, B.; Kosztin, D.; Lu, H.; Molnar, F.; Wriggers, W.; Schulten, K. Steered Molecular Dynamics. In *Computational Molecular Dynamics: Challenges, Methods, Ideas*; Deuflhard, P., Hermans, J., Leimkuhler, B., Mark, A., Reich, S., Skeel, R., Eds.; Springer: Berlin, 1999; Vol. *4*, pp 39−65.
(24) Vilatela, J. J.; Windle, A. H. Yarn-like carbon nanotube fibers. *Adv. Mater.* **2010**, *22* (44), 4959−4963.
(25) Motta, M.; Moisala, A.; Kinloch, I. A.; Windle, A. H. High performance fibres from 'dog bone' carbon nanotubes. *Adv. Mater.* **2007**, *19* (21), 3721−3726.
(26) Xiang, C.; Young, C. C.; Wang, X.; Yan, Z.; Hwang, C.-C.; Cerioti, G.; Lin, J.; Kono, J.; Pasquali, M.; Tour, J. M. Large flake graphene oxide fibers with unconventional 100% knot efficiency and highly aligned small flake graphene oxide fibers. *Adv. Mater.* **2013**, *25* (33), 4592−4597.
(27) Walsh, R. B.; Nelson, A.; Skinner, W. M.; Parsons, D.; Craig, V. S. J. Direct measurement of van der Waals and diffuse double-layer forces between titanium dioxide surfaces produced by atomic layer deposition. *J. Phys. Chem. C* **2012**, *116* (14), 7838−7847.
(28) Loskill, P.; Hähl, H.; Faidt, T.; Grandthyll, S.; Müller, F.; Jacobs, K. Is adhesion superficial? Silicon wafers as a model system to study van der Waals interactions. *Adv. Colloid Interface Sci.* **2012**, *179*−*182*, 107−113.
(29) Kamperman, M.; Kroner, E.; del Campo, A.; McMeeking, R. M.; Arzt, E. Functional adhesive surfaces with "gecko" effect: the concept of contact splitting. *Adv. Eng. Mater.* **2010**, *12* (5), 335−348.
(30) Xia, Z.; Curtin, W. A. Pullout forces and friction in multiwall carbon nanotubes. *Phys. Rev. B* **2004**, *69* (23), 233408.
(31) Johnson, R. R.; Johnson, A. T. C.; Klein, M. L. Probing the structure of DNA−carbon nanotube hybrids with molecular dynamics. *Nano Lett.* **2008**, *8* (1), 69−75.
(32) Shibuta, Y.; Elliott, J. A. Interaction between two graphene sheets with a turbostratic orientational relationship. *Chem. Phys. Lett.* **2011**, *512* (4−6), 146−150.
(33) Zhang, S.; Mielke, S. L.; Khare, R.; Troya, D.; Ruoff, R. S.; Schatz, G. C.; Belytschko, T. Mechanics of defects in carbon nanotubes: atomistic and multiscale simulations. *Phys. Rev. B* **2005**, *71* (11), 115403.
(34) Nardelli, M. B.; Yakobson, B. I.; Bernholc, J. Brittle and ductile behavior in carbon nanotubes. *Phys. Rev. Lett.* **1998**, *81* (21), 4656−4659.
(35) Koziol, K.; Vilatela, J.; Moisala, A.; Motta, M.; Cunniff, P.; Sennett, M.; Windle, A. High-performance carbon nanotube fiber. *Science* **2007**, *318* (5858), 1892−1895.